CRYSTAL GROWTH

Tetracene Crystals: Growth from Solutions, Solubility, and Thermal Properties

A. A. Kulishov[a],*, G. A. Yurasik[a], V. V. Grebenev[a], and V. A. Postnikov[a],**

[a] Shubnikov Institute of Crystallography, Federal Scientific Research Centre "Crystallography and Photonics,"
Russian Academy of Sciences, Moscow, 119333 Russia
*e-mail: adakyla1255@gmail.com
**e-mail: postva@yandex.ru

Abstract—The solubility of tetracene crystals has been investigated experimentally and theoretically within the approximation of regular-solution model. The grown crystals had a shape of thin elongated plates. The largest tetracene crystal (8 mm × 50 μm in size) was grown from a benzene solution by precipitant vapor diffusion into solution. The X-ray diffraction pattern from a developed crystal face is the result of the X-ray beam reflection from the (001) plane of a set of monolayers with a thickness $d_{001} = 1.21$ nm. An analysis of the surface morphology of the (001) face of tetracene crystal by atomic force microscopy (AFM) revealed the presence of elementary growth steps, whose height coincides (within the measurement error) with the monolayer thickness d_{001}. The parameters of melting ($T_m = 343.0°C$, $\Delta H_m = 35.6$ kJ/mol) and polymorphic transition ($T_{tr} = 310.0°C$, $\Delta H_{tr} = 0.9$ kJ/mol) of tetracene were refined using differential scanning calorimetry (DSC). A comparison of the optical absorption and luminescence spectra of solutions of a pure tetracene sample and a processed (previously molten in a hermetic crucible in an inert atmosphere) sample in toluene confirms degradation of the material subjected to overheating above the melting temperature.

INTRODUCTION

Tetracene (Tc) is a polycyclic aromatic hydrocarbon, consisting of four linearly condensed aromatic rings. The Tc crystal structure was investigated for the first time in 1936 by single-crystal X-ray diffraction, as a result of which its triclinic symmetry was revealed and lattice parameters were determined [1–3].

Tc crystals are of great interest as efficient *p*-type organic semiconductors; their electrical properties have been studied for more than 50 years [4–7]. Tc crystals are applied as active layers when designing electronic and optoelectronic devices, such as field-effect [8–16] and light-emitting [17, 18] transistors.

One of the simplest ways to form thin crystalline Tc films in the composition of organic field-effect transistors (OFET) in order to study electrical properties is thermal vacuum deposition [6, 8, 19, 20]. Crystalline films obtained by this technique are uniform in thickness; however, they are characterized by low structural quality: they are in fact polycrystals with a characteristic average grain size on the order of several hundreds of nanometers.

Currently, because of the low solubility of Tc crystals, the main way to synthesize centimeter-sized (0.2–2 cm) Tc single crystals is physical vapor transport (PVT) [21–24]. The crystals grown in this way are wide films or plates, whose basal face is oriented in the (001) plane. For these crystals, the shape anisotropy factor (defined as the thickness-to-length ratio) lies in the range of 10^{-3}–10^{-5}.

There are data on the synthesis of a bulky, conically shaped (2 cm long) Tc single crystal by the vapor Bridgman method [25]. This sample contained many linear defects: cracks, oriented in the [100] direction, which approximately coincided with the conical axis of the crystal.

The PVT-grown flat Tc single crystals in the composition of field transistors, due to their high structural quality and minimum number of structural defects, exhibit the best electrical properties with a maximum hole mobility, reaching 1.0 cm^2 V^{-1} s^{-1} at room temperature [7, 9–12].

Nevertheless, the methods for growing crystals of organic π-conjugated molecules from solutions are of great interest in view of their wide possibilities in scaling and in situ monitoring the growth process in comparison with the PVT methods. Unfortunately, the data in the literature on the growth of Tc crystals from solutions are fairly scarce, and there are barely any data on the growth of centimeter-sized crystalline samples. The data in the literature on the Tc solubility are also scarce [26, 27].

Despite the low solubility, relatively large single crystals of π-conjugated organic molecules can be grown from solutions in some cases. In particular, results on growing centimeter-sized (0.2−1 cm) single crystals from solutions were reported recently for some linear molecules with a number of π-conjugated units $n \geq 4$ [28−32].

The purpose of this work was to investigate the solubility of tetracene crystals and their growth from solutions, as well as to analyze their phase behavior upon heating by differential scanning calorimetry (DSC).

EXPERIMENTAL

Materials

The object of study was tetracene (98%) produced by Sigma-Aldrich. Toluene of special-purity grade and benzene of analytical grade were used as solvents and solvophobic alcohols (isopropyl alcohol of analytical grade and butanol-1 of analytical grade) were used as precipitants. The choice of solvents for the crystal growth is determined by the existence of data on the solubility of tetracene in them at room temperature [26, 27]. In addition, according to the existing experience in this field, the aforementioned solvents have proven to be fairly efficient for growing crystals of organic π-conjugated linear molecules from solutions [29−33].

Differential Scanning Calorimetry

The thermal properties of crystals were investigated in the temperature range of 25−375°C on a thermoanalytical complex STA Netzsch 449 F1. Experiments performed in hermetic aluminum crucibles in a nitrogen atmosphere. The rate of temperature variation was 5 K/min. Calibration of thermal sensitivity was performed using a sample of single-crystal sapphire, with subsequent calculation of the sensitivity curve for the system. The experimental data were processed within the NETZSCH Proteus Thermal Analysis program.

Solubility and Growth of Crystals

The solubility C_{m} of tetracene in benzene and in toluene at 20°C was found using the method for determining the fraction of dry precipitate when drying a saturated solution in a volume of 20 mL. The initial saturated solution and the dry residue were weighted on an analytical balance AUW-220D (Shimadzu, Japan) with a maximum permissible error of ±0.1 mg (accuracy class according to GOST (State Standard) 24104-I). The solubility of Tc in toluene at 50°C was determined using the method for monitoring undissolved precipitate during long-term isothermal exposure of solution. Crystalline Tc samples were grown from solution by the solvent−precipitant method,

which ensures slow diffusion of solvophobic solvent−precipitant from the vapor phase through the liquid−air interface into the solution [30−33]. Crystal growth occurred both on the liquid-air interface and on the vessel bottom. To make the material dissolve completely, solutions were processed in an ultrasonic bath. After cooling to room temperature solutions were filtered using a disposable polytetrafluoroethylene filter with a pore size of 0.2 μm and poured into a 50-mL measuring glass vessel, which was then placed in a hermetic glass growth chamber with a precipitant previously poured on the bottom. Then the chamber with a Tc solution was kept in a thermostat at 20°C. After the end of the growth period several large crystalline samples were found in the solution bulk. Some crystals formed at the liquid−air interface, while growing, precipitated on the bottom as a result of dominance of their weight over the surface tension (the crystal density exceeds the solution density), where their further growth occurred.

Optical Microscopy and Atomic-Force Microscopy

The surface morphology and thickness of grown crystalline Tc films were investigated with a confocal microscope LEXT OLS 3100 (Olympus, Japan) and an atomic-force microscope (AFM) Ntegra (NT-MDT, Russia) in the tapping mode (NSG01 probes with a cantilever rigidity of 5.1 N/m, resonant frequency of 103 kHz, and a tip radius of no more than 10 nm), calibrated in the horizontal plane using a TGZ1 sample (NT-MDT). Measurements along the z coordinate were calibrated using elementary steps on the basal face of a potassium mica crystal, formed by treating its fresh cleavage in a 50% aqueous solution of hydrofluoric acid [34]. The AFM topographs were processed and analyzed using the Gwyddion program [35].

X-Ray Diffraction Analysis

The structure of the largest crystals was investigated on an X-ray powder diffractometer Miniflex 600 (Rigaku, Japan) (radiation CuK_{α}, $\lambda = 1.54178$ Å, scan rate 2 deg/min). Crystal samples were previously fixed on a quartz substrate by a drop of alcohol; X-ray diffraction reflection was recorded from the most developed flat surface of crystals.

Optical Absorption and Luminescence Spectra

Spectral analysis of the solutions in toluene was performed for several Tc samples: a singly recrystallized one (1) and samples previously subjected to thermal treatment during DSC experiments upon heating above the polymorphic transition temperature to 325°C (2) and above the melting temperature (3). Solutions with a concentration of ~0.1 g/L were prepared. Their absorption and luminescence spectra were measured in a quartz cell (optical path 1 cm)
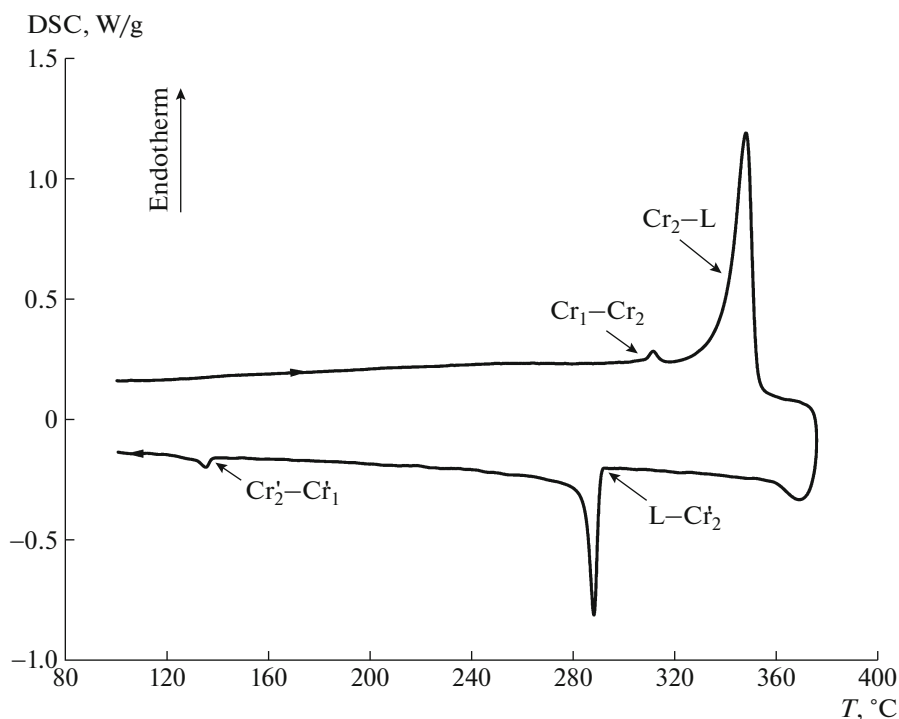
Fig. 1. DSC curve for tetracene.

RESULTS AND DISCUSSION

Differential Scanning Calorimetry

The DSC curve, characterizing the thermal behavior of Tc, is presented in Fig. 1. The found phase-transition parameters are listed in Table 1. Two endothermic peaks were revealed upon heating Tc samples: a small peak at a temperature $T_{tr} = 310.0 \pm 0.1°C$ with an enthalpy $\Delta H_{tr} = 0.9 \pm 0.1$ kJ/mol (Cr_1-Cr_2) and a large peak at a temperature $T_m = 343.0 \pm 0.1°C$ with an enthalpy $\Delta H_m = 35.6 \pm 0.5$ kJ/mol (Cr_2-L), which are due to the polymorphic phase transition and melting, respectively. Upon cooling the Tc melt is crystallized at a temperature much lower than the melting point T_m ($L-Cr_2'$), with a supercooling $\Delta T_m = 50-60°C$. A weak exothermic transition is observed at a temperature 137°C ($Cr_2'-Cr_1'$). However, if the sample is not heated to the melting temperature T_m in the first heating cycle, an inverse exothermic transition from the high- to low-temperature crystalline phase with a temperature hysteresis of ~0.5°C is observed upon cooling. According to the data of [36, 37], a

polymorphic transition of Tc was observed in the range of 308−309°C, and the melting temperature was 7 to 10°C higher than the value determined under given conditions (Table 1). The inconsistency in the melting temperatures may be related to the difference in the compositions of the inert atmosphere in which crucibles were sealed. It was indicated in [36] that Tc decomposes upon melting, which affects the accuracy of determining the melting enthalpy ΔH_m. It was also found that Tc undergoes partial chemical degradation during melting, as is evidenced by the irreproducibility of the results obtained in the second and subsequent heating cycles, as well as the results of comparing (see below) the absorption spectra of the solutions of the initial material and the samples heated to temperatures below and above T_m. Correspondingly, the endothermic peak related to the sample melting also contains a contribution from the Tc degradation processes. We could not separate these contributions and select the contribution from melting in our experiments. Therefore, the error found for the heat of fusion is related to only the error in determining the peak area for a series of experiments, and the true melting enthalpy of this compound is lower.

Absorption and Luminescence Spectra of Solutions

Figure 2 shows the normalized absorption (solid curves) and luminescence (dotted curves) spectra of the solutions of singly recrystallized Tc in toluene (curves *1*) and the samples subjected to heating slightly

Table 1. Parameters of the phase transitions in tetracene crystals

References	Crystal II → crystal I		Crystal I → liquid	
	T_{tr}, °C	ΔH_{tr}, kJ/mol	T_m, °C	ΔH_m, kJ/mol
This study	310.0 ± 0.1	0.9 ± 0.1	343.0 ± 0.1	35.6 ± 0.5
[36]	308.8	1.2	353.1	36.8
[37]	308.3	1.0	350.1	35.9

above the polymorphic transition temperature (to 325°C) (curves *2*) and overheated above the melting temperature T_m (curves *3*). It can be seen in Fig. 2 that the absorption and luminescence spectra of the solution of initial Tc (curve *1*) coincide in shape with the spectra reported in [38]. The spectra of Tc heated to 325°C (curve *2*) coincide with the spectra of pure Tc in the visible region and somewhat differ in the UV range. The difference in the absorption spectra of the solutions of pure Tc and Tc heated to 325°C (curve δ_{12}) decreases with an increase in wavelength according to the law characteristic of the Rayleigh scattering spectrum. This fact indicates that the solution of this sample contains, along with the tetracene monomer, some scattering particles, which are likely due to the partial degradation of material.

The absorption spectrum of the solution of Tc sample (curve *3*) overheated above T_m is barely structured; as well as the above-described difference spectrum δ_{12}, it has a shape characteristic of Rayleigh scattering spectrum. At the same time, one can trace a weakly pronounced vibrational structure of monomer spectrum. The recorded emission spectrum of this solution differs significantly from the spectrum of Tc monomer and contains artifacts related to the excitation light scattering. The above-described spectral features are indicative of significant chemical changes occurring in the composition of the Tc sample subjected to melting, thus confirming the effect of material degradation.

Solubility, Growth, and Surface Morphology of Crystals

The obtained data on the solubility C_m of tetracene at 20°C in benzene and toluene are listed in Table 2. One can see that the C_m values found under given conditions differ significantly from the data in the literature. An analysis showed that the solubility of Tc in toluene at 50°C is $C_m = 2.0 ± 0.2$ g/L.
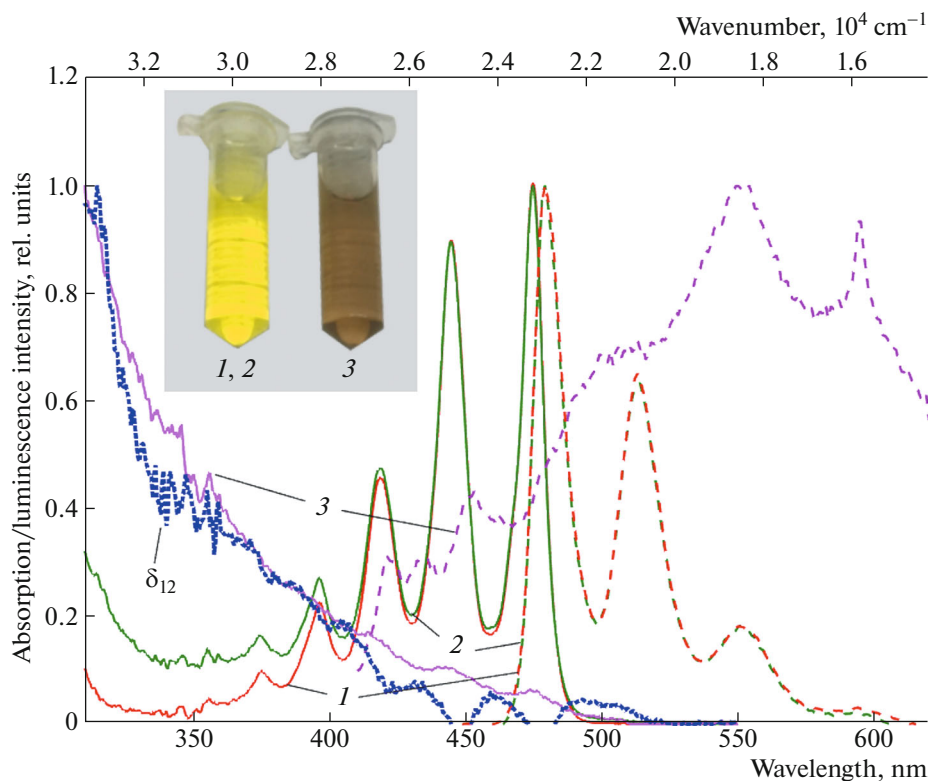

Fig. 2. Normalized absorption (solid lines) and luminescence (dashed lines) spectra of solutions of tetracene samples: (*1*) singly recrystallized tetracene and (*2*, *3*) samples subjected to heating (*2*) to 325°C and (*3*) above the melting temperature; (δ_{12}) is the normalized difference of absorption spectra (*1*, *2*). The inset shows images of test tubes with concentrated solutions (*1*, *3*); the color of solution (*2*) was identical to that of solution (*1*).

Table 2. Characteristics of tetracene crystal growth from solutions at 20°C

Solvent	C_m, g/L	Precipitant	T, days	C_0, g/L	L_{max}, mm	H_{max}, μm	V_L, μm/h
Benzene	0.6 ± 0.1	Isopropyl alcohol	7	0.2	8	50	48
	2.2 [26]	Butanol-1	4	0.25	1.5	19	16
Toluene	0.5 ± 0.1	Isopropyl alcohol	7	0.2	4	10	24
	0.16 [27]						

C_m is the saturated-solution concentration; T is the growth time; C_0 is the initial solution concentration; L_{max} and H_{max} are, respectively, the maximum length and thickness of crystals; and V_L is the average linear growth rate of the largest crystals.

The data on the solubility C_m of linear acenes in toluene at 20°C, with allowance for the obtained value for Tc, are presented as a semilogarithmic dependence on the number n of aromatic rings in Fig. 3. The data on naphthalene and anthracene were taken from [39, 40]. One can see that the dependence of the solubility of linear acene molecules on the number n of conjugated rings is interpolated fairly well by the exponential dependence

$$C_m = a_1 \exp(-a_2 n), \quad (1)$$

where $a_1 = (488 \pm 12) \times 10^3$ and $a_2 = 3.538 \pm 0.013$ ($R^2 = 1$). Extrapolating this dependence to $n = 5$, one can estimate the solubility in toluene for the next term in the homologous series of acenes, pentacene, as $C_m = 0.01$ g/L (open circle in Fig. 3).

In the regular-solution approximation based on the Scatchard–Hildebrandt model [41], using the found values of solubility in toluene at 20°C and tetracene melting parameters $T_{m,2}$ and $\Delta H_{m,2}$ (Table 1), as well as the values of molar volumes $V_{m,i}$ of both solution components ($V_{m,1} = M_1/\rho_1 = 106.3 \times 10^{-6}$ m^3 mol^{-1} for toluene [42] and $V_{m,2} = M_2/\rho_2 = 172.6 \times 10^{-6}$ m^3 mol^{-1} for Tc [43]; ρ_i is the crystal density), a model was constructed for the curve of tetracene solubility T_s in toluene:

$$T_s = (\Delta H_{m,2} + V_{m,2}\varphi_1^2 A)/(\Delta H_{m,2}/T_{m,2} - R\ln X_2), \quad (2)$$

where $\varphi_1 = (X_1 V_{m,1})/(X_1 V_{m,1} + X_2 V_{m,2})$ is the volume fraction of the solvent; X_1 and X_2 are the molar fractions of the solvent and solute, respectively; R is the universal gas constant; and A is a parameter determining the coefficient of Tc activity in solution, which is found using Eq. (2) via the known concentration of saturated solution at 20°C. The dependence of T_s on the molar solubility C_M (solid line) is shown in Fig. 4.
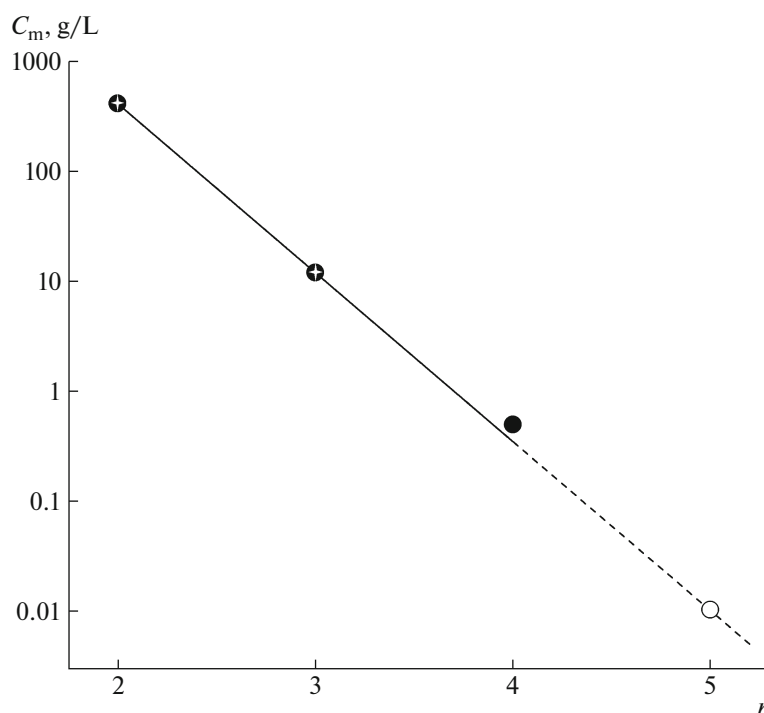
Fig. 3. Dependence of the solubility of linear acenes in toluene at 20°C on the number n of conjugated rings.
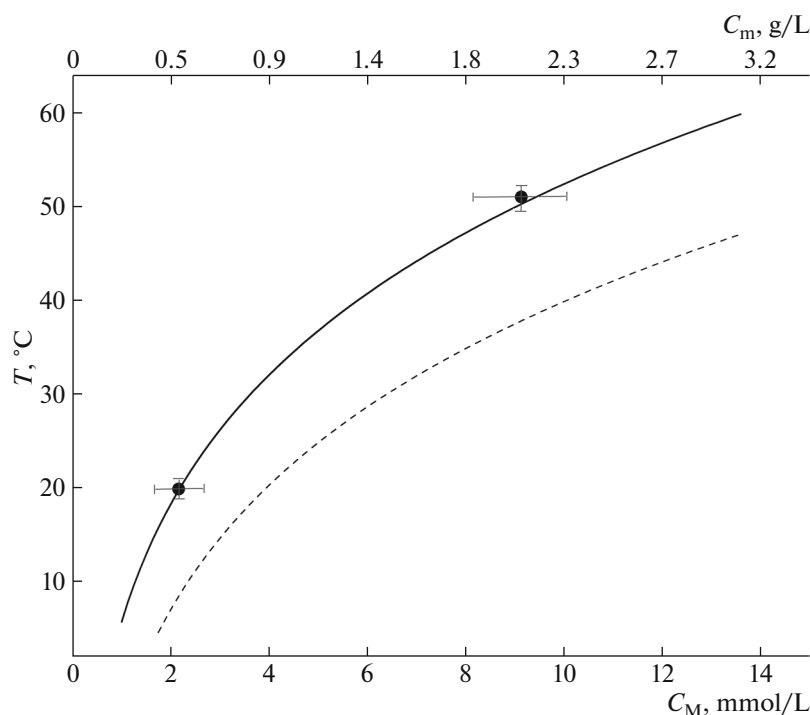
Fig. 4. Curves of tetracene solubility in toluene, plotted in the approximations of regular (solid line) and ideal (dashed line) solutions. Points are experimentally found values.

Recalculation into units of mass concentration C_m is given on the upper abscissa scale. It can be seen that the solubility curve plotted within the regular-solution approximation is in agreement (within the error) with the value found for 50°C. For comparison, the dashed line in Fig. 4 shows the solubility curve calculated within the ideal-solution approximation (Schröder–van Laar model) [41], which deviates significantly from the experimental points.

The results on growing Tc crystals are given in Table 2. The best growth characteristics were observed for the growth from a benzene solution in an atmosphere saturated with isopropyl alcohol vapor. The largest Tc crystal grown under these conditions has a lamellar shape with an area of 8×1 mm^2 and a thickness of ~50 μm (Fig. 5a). The crystal growth in toluene solutions occurred more slowly. In this case the largest crystals had a needle-like shape and reached 4 mm in length; their width and length did not exceed 150 and 50 μm, respectively (Fig. 5b). Enlarged images of crystals grown from benzene and toluene solutions are presented in Figs. 5c and 5d, respectively. It can be seen that the lateral sides of flat crystals are faceted. The following characteristic angles were observed between the lateral faces: 104°, 125°, 130°, and 135° (Figs. 5c, 5d).

The wide face of tetracene crystals has generally a developed surface morphology, characterized by the presence of macrosteps and some texture (Fig. 5c). Crystals with a smoother surface are also observed

(Fig. 5d). Figure 6 shows an AFM surface topograph for one of these crystals. This image exhibits the presence of elementary growth steps with a height $h_0 = 1.3 \pm 0.1$ nm (the cross section profile is shown in Fig. 6). The found h_0 value is in agreement with the result reported in [44] for a crystal grown from the vapor phase.

X-Ray Diffraction and Crystal Structure of Crystals

The X-ray diffraction pattern of a flat Tc single crystal, recorded in reflection from the developed face, is shown in Fig. 7 (the line height is normalized to maximum). These results are in good agreement with the structural data reported in [43]. The calculated powder diffraction pattern from the aforementioned study is shown for comparison in Fig. 7 (bottom). It can be seen that the spectrum of diffraction reflections for the crystal studied is generally a set of narrow peaks, whose positions are approximately multiples of the position of the first peak at $2\theta_1 = 7.28°$ and correspond to the reflection from a set of monolayers parallel to (001) planes. A calculation by the Bragg formula gives the following value of interplanar spacing for this set of planes: $d_{001} = 1.21$ nm.

The elementary step height h_{001} on the (001) face, found by the AFM method (Fig. 6), is almost 8% higher than the interplanar spacing d_{001} determined in the X-ray-diffraction experiment; however, taking
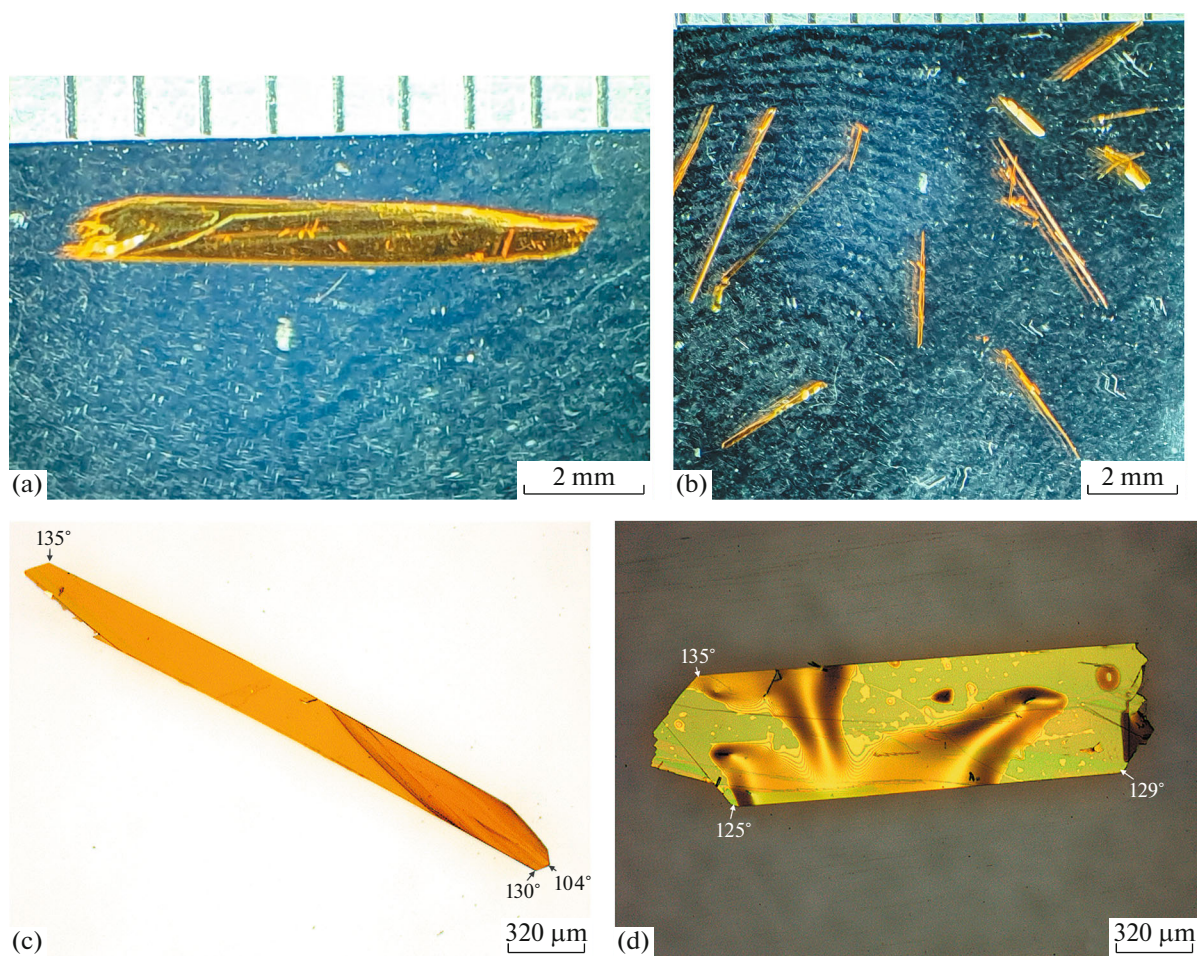
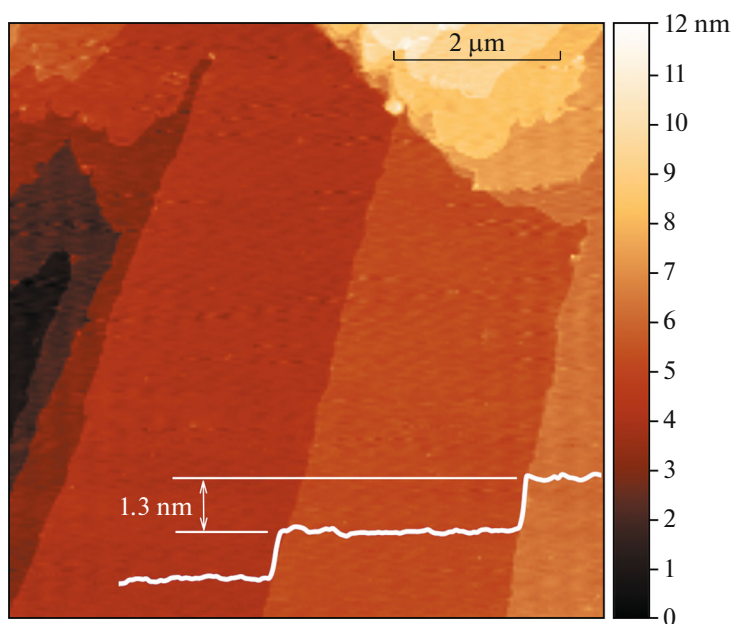**Fig. 5.** Tetracene crystals grown from (a, c) benzene and (b, d) toluene solutions.

Fig. 6. Topographic image of an area of tetracene crystal surface with a horizontal cross section profile (white line).
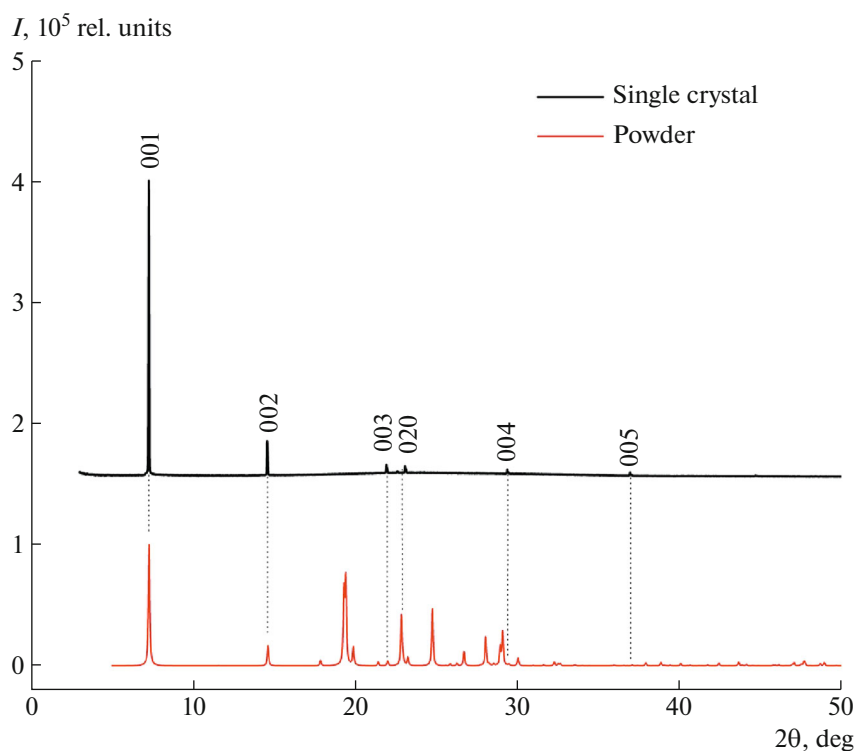
I, 10^5 rel. units

Fig. 7. X-ray diffraction patterns of tetracene single crystal and tetracene powder [43].

into account the larger error of the probe method, one can speak about correspondence of the monolayer thicknesses determined by these methods.

Let us consider the Tc crystal structure based on the results reported in [43], using data visualization within the Mercury software package [45]. At room and low temperatures the Tc crystal structure is characterized by the triclinic symmetry $P\bar{1}$ with $Z = 2$. The unit-cell parameters are $a = 6.0565(9)$ Å, $b = 7.8376(11)$ Å, $c = 13.0104(18)$ Å; $\alpha = 77.127(2)°$, $\beta = 72.118(2)°$, $\gamma = 85.792(2)°$. A view of the crystal unit cell is presented in Fig. 8a. The X-ray diffraction density of the crystal is $\rho_0 = 1.323$ g/cm^3. The Tc crystal has a layered structure in the form of a stack of monolayers oriented parallel to the (001) plane (Fig. 8a). The thickness of an individual monolayer is $d_{001} = 1.210$ nm. The molecular axis makes an angle $\chi = 70.0°$ with the (001) plane (Fig. 8a). Inside the monolayers in the (001) orientation molecules are packed into a herringbone structure with a herringbone angle $\theta = 50.1°$ (Fig. 8b). The shortest intermolecular bond is implemented in the [110] direction, and the most closely packed rows of molecules are oriented in the [100] direction (Fig. 8b). Planar Tc molecules are oriented parallel to either (256) or $(\bar{4}\ 12\ 5)$ planes in the crystal (Fig. 8b). Specifically the angle between these planes determines the angle θ (Fig. 8b). Let us select a compact cluster of molecules, limited by the (010),

$(0\bar{1}0)$, (110), $(1\bar{1}0)$, $(\bar{1}\bar{1}0)$, and $(\bar{1}10)$ planes, in a monolayer in the (001) orientation, as shown in Fig. 8c. As one can see, there are angles of 104.65°, 125.04°, and 130.31° between the sides of the newly formed hexagon. The planar figure obtained in this way presents the shape of an ideal Tc crystal with the corresponding faceting of lateral sides in the projection on the (001) plane. Having compared the angles between the lateral sides of the ideal shape (Fig. 8c) and the real crystal, one can determine the indices of the lateral faces of real crystal, presented as an example in Fig. 8d. It can be seen that the faces with indices (010), (110), and $(1\bar{1}0)$ and the preferred growth direction [100] are easily identified for this crystal.

To explain the fastest growth of Tc crystal in the [100] direction, we will consider the model of pair interactions between the nearest molecules in a monolayer with the (001) orientation, using the UNI Intermolecular Potentials algorithm, built-in into the Mercury software package. A schematic of the interaction between the central molecule (0) and its nearest neighbors (1–6) is presented in Fig. 9. The algorithm in use determines the pair-interaction potentials (blue numbers in kJ/mol in Fig. 9) and the distances between centers (black numbers in Å in Fig. 9) of the aforementioned molecules, based on structural data. Let us consider a two-dimensional microscopic model of the force interaction of the central molecule,
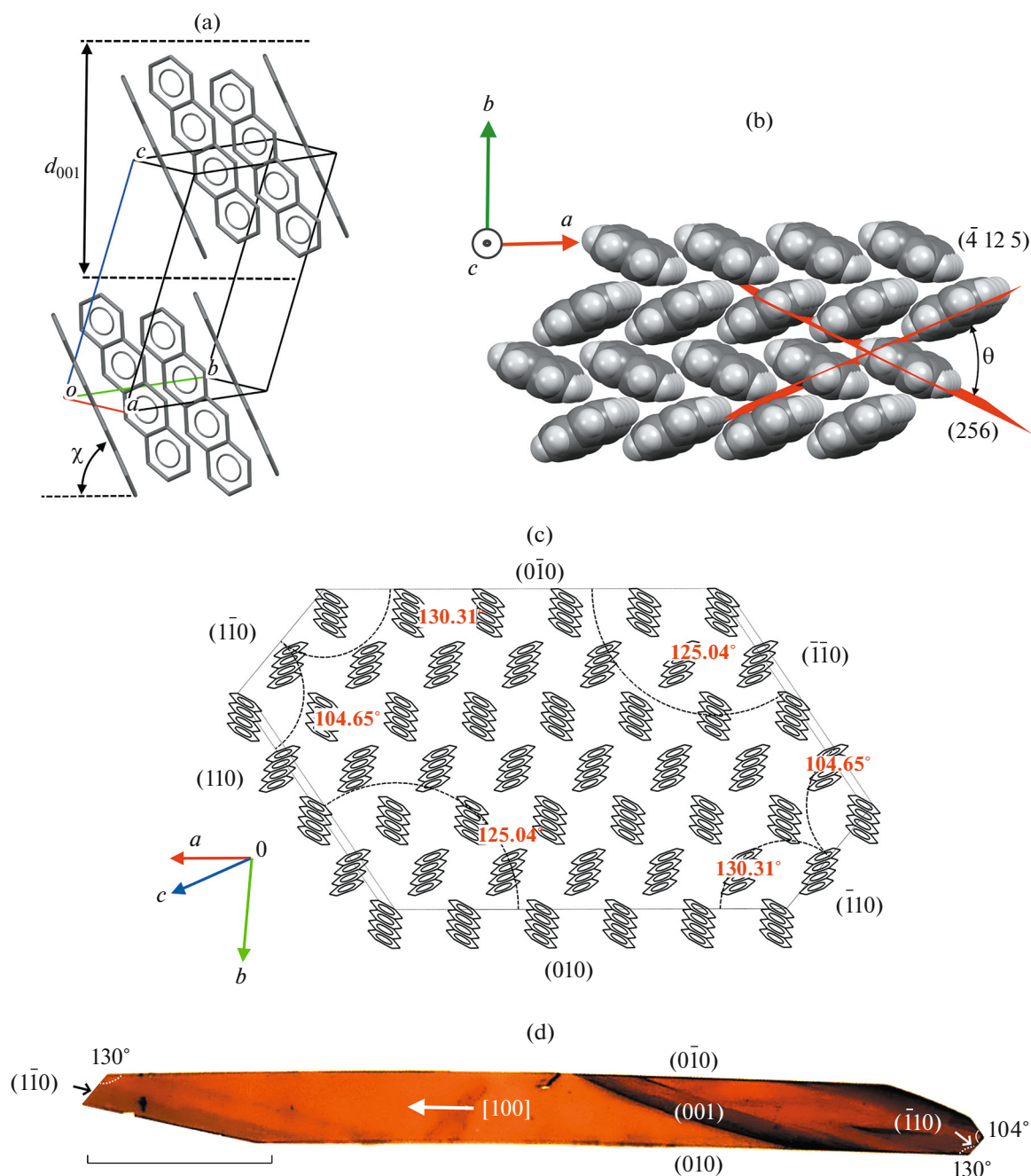
Fig. 8. Tetracene crystal structure at 20°C: (a) view of the unit cell, (b) schematic diagram of molecular packing in a monolayer parallel to the (001) plane, (c) element of crystalline monolayer parallel to the (001) plane and limited by some low-index planes, and (d) optical image of crystal with symbols of faces (0.5-mm scale).

located in a certain linear molecular row, with the nearest environment beyond this row (the lateral intermolecular bonds between molecules in the (001) plane). The green numbers in the scheme indicate the angles between the central molecule (0) and some directions interesting for us.

The resulting force of interaction of the central molecule with molecules *1, 2,* and *6* in the $[1\bar{1}0]$ direction can be written as

$$F_{[1\bar{1}0]} = -\left[\frac{U_{01}}{r_{01}} + \frac{U_{06}}{r_{06}}\cos(\widehat{601}) + \frac{U_{02}}{r_{02}}\cos(\widehat{102})\right], \quad (3)$$
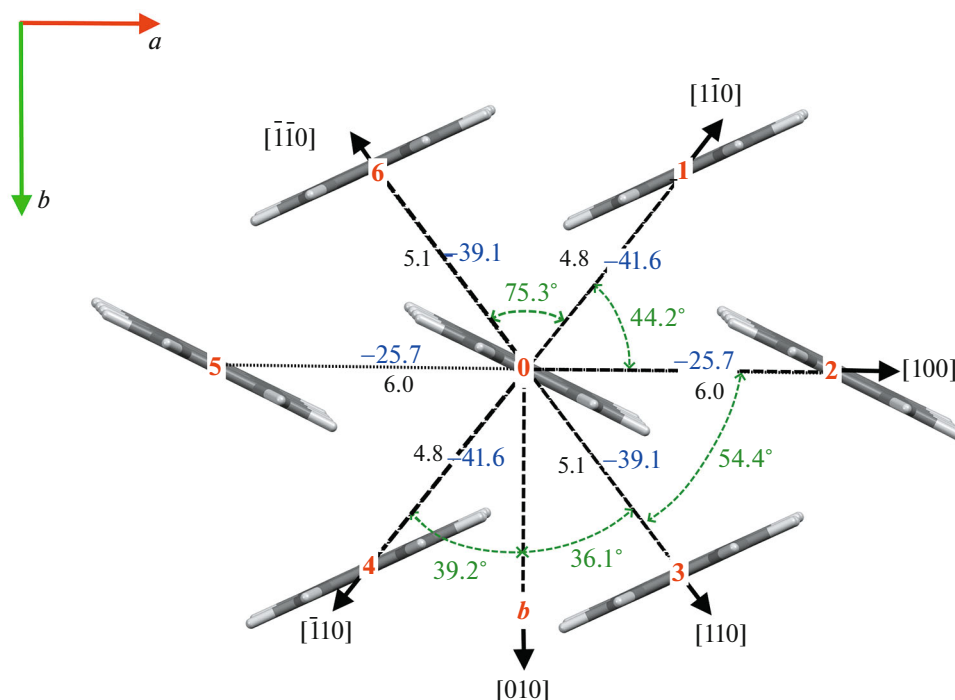
Fig. 9. Schematic of pair interactions between nearest tetracene molecules in a (001) monolayer. Black and blue numbers indicate, respectively, the distances between the centers of neighboring molecules (in Å) and the pair-interaction potentials (in kJ/mol); the angles between the aforementioned directions are denoted by green numbers.

where U_{0i} and r_{0i} are, respectively, the pair potential and the distance between the centers of molecules 0 and i; $\widehat{601}$ and $\widehat{102}$ are the angles between the centers of the corresponding molecules. In a similar way we will determine the resulting constraint forces between molecule 0 and the nearest neighbors in the [100], [010], and [110] directions:

$$F_{[100]} = -\left[\frac{U_{02}}{r_{02}} + \frac{U_{01}}{r_{01}}\cos(\widehat{102}) + \frac{U_{03}}{r_{03}}\cos(\widehat{203})\right], \quad (4)$$

$$F_{[010]} = -\left[\frac{U_{03}}{r_{03}}\cos(\widehat{30b}) + \frac{U_{04}}{r_{04}}\cos(\widehat{40b})\right], \quad (5)$$

$$F_{[110]} = -\left[\frac{U_{03}}{r_{03}} + \frac{U_{02}}{r_{02}}\cos(\widehat{203}) + \frac{U_{04}}{r_{04}}\cos(\widehat{403})\right]. \quad (6)$$

Substitution of the numerical values of the corresponding parameters (see Fig. 9) into expressions (3)–(6) yields the largest resulting interaction force between the central molecule and its environment in the [100] direction, $F_{[100]}$:

$$\frac{F_{[100]}}{F_{[010]}} = 1.163, \quad \frac{F_{[100]}}{F_{[110]}} = 1.210, \quad \frac{F_{[100]}}{F_{[1\bar{1}0]}} = 1.095.$$

Thus, the simple model estimation based on the data on pair-interaction potentials indicates the presence of the strongest resulting interaction between the nearest molecules in the [100] direction, which, apparently, provides the maximum growth rate of Tc crystal in this direction.

CONCLUSIONS

The results of the theoretical study of tetracene solubility in toluene within the approximation of regular-solution model showed good agreement with the experimental data. Despite the low solubility at room temperature, the solution technique nevertheless allows one to grow centimeter-sized Tc single crystals; this format is quite favorable for a comprehensive study of the structural and morphological characteristics, as well as the optoelectronic properties, on one sample. The Tc crystals grown from solutions have a shape elongated in the [100] direction and are generally laterally faceted. A model estimation based on the data on pair-interaction potentials showed that the resulting interaction force between the nearest molecules of monolayer in the (001) orientation is maximum in the projection on the [100] direction, a circumstance apparently motivating the preferred crystal growth in this direction. The best growth characteristics were revealed for the crystals grown from benzene solutions. The found value of the polymorphic transition temperature, $T_{tr} = 310°C$, is in good agreement with the data in the literature. However, the melting

temperature determined by us (T_m = 343°C) turned out to be from 7 to 10 K below the values reported in the literature, which may be related to the specificity of experiments in hermetic crucibles and the use of different inert gases as growth atmospheres.

FUNDING

CONFLICT OF INTEREST

The authors declare that they have no conflicts of interest.

REFERENCES

1. E. Hertel and H. W. Bergk, Z. Phys. Chem. B **33**, 319 (1936).
https://doi.org/10.1515/zpch-1936-3329

2. J. M. Robertson, V. C. Sinclair, and J. Trotter, Acta Crystallogr. **14** (7), 697 (1961).
https://doi.org/10.1107/s0365110x61002151

3. R. B. Campbell, J. M. Robertson, and J. Trotter, Acta Crystallogr. **15** (3), 289 (1962).
https://doi.org/10.1107/s0365110x62000699

4. M. Pope, J. Burgos, and J. Giachino, J. Chem. Phys. **43** (9), 3367 (1965).
https://doi.org/10.1063/1.1726399

5. A. Szymanski and M. M. Labes, J. Chem. Phys. **50** (4), 1898 (1969).
https://doi.org/Pj10.1063/1.1671293

6. W. Mycielski and A. Lipiński, Thin Solid Films **48** (2), 133 (1978).
https://doi.org/10.1016/0040-6090(78)90235-3

7. J. H. Schön, C. Kloc, and B. Batlogg, Phys. Rev. Lett. **86** (17), 3843 (2001).
https://doi.org/10.1103/PhysRevLett.86.3843

8. D. J. Gundlach, J. A. Nichols, L. Zhou, et al., Appl. Phys. Lett. **80** (16), 2925 (2002).
https://doi.org/10.1063/1.1471378

9. V. Y. Butko, X. Chi, and A. P. Ramirez, Solid State Commun. **128** (11), 431 (2003).
https://doi.org/10.1016/j.ssc.2003.08.041

10. R. W. I. De Boer, T. M. Klapwijk, and A. F. Morpurgo, Appl. Phys. Lett. **83** (21), 4345 (2003).
https://doi.org/10.1063/1.1629144

11. X. Yu, V. Kalihari, C. D. Frisbie, et al., Appl. Phys. Lett. **90** (16), 2005 (2007).
https://doi.org/10.1063/1.2724895

12. C. R. Newman, R. J. Chesterfield, J. A. Merlo, et al., Appl. Phys. Lett. **85** (3), 422 (2004).
https://doi.org/10.1063/1.1771466

13. T. H. Kim, J. H. Lee, J. H. Kim, et al., Mater. Res. Soc. Symp. Proc. **920**, 39 (2006).
https://doi.org/10.1557/proc-0920-s02-04

14. R. W. I. De Boer, M. Jochemsen, T. M. Klapwijk, et al., J. Appl. Phys. **95** (3), 1196 (2004).
https://doi.org/10.1063/1.1631079

15. R. J. Tseng, R. Chan, V. C. Tung, et al., Adv. Mater. **20**, 3 (2008).
https://doi.org/10.1002/adma.200701374

16. H. J. Jang, E. G. Bittle, Q. Zhang, et al., ACS Nano **13** (1), 616 (2019).
https://doi.org/10.1021/acsnano.8b07625

17. C. Santato, R. Capelli, M. A. Loi, et al., Synth. Met. **146** (3), 329 (2004).
https://doi.org/10.1016/j.synthmet.2004.08.028

18. T. Takahashi, T. Takenobu, J. Takeya, and Y. Iwasa, Adv. Funct. Mater. **17** (10), 1623 (2007).
https://doi.org/10.1002/adfm.200700046

19. P. S. Abthagir, Y. G. Ha, E. A. You, et al., J. Phys. Chem. B **109** (50), 23918 (2005).
https://doi.org/10.1021/jp054894r

20. G. Luka, L. Nittler, E. Lusakowska, et al., Org. Electron. **45**, 240 (2017).
https://doi.org/10.1016/j.orgel.2017.03.031

21. C. Kloc, P. G. Simpkins, T. Siegrist, et al., J. Cryst. Growth **182** (3) (1997).
https://doi.org/10.1016/S0022-0248(97)00370-9

22. H. Wang, Y. Zhao, Z. Xie, et al., CrystEngComm **16** (21) (2014).
https://doi.org/10.1039/c3ce42367k

23. R. Laudise, C. Kloc, P. G. Simpkins, et al., J. Cryst. Growth **187** (3–4), 449 (1998).
https://doi.org/10.1016/S0022-0248(98)00034-7

24. R. L. Lidberg, PhD Thesis (University of Minnesota, 2017).

25. J. Niemax and J. Pflaum, Appl. Phys. Lett. **87**, 241921 (2005).
https://doi.org/10.1063/1.2146072

26. S. M. Leshchev and A. V. Sin'kevich, Zh. Prikl. Khim. **9** (9), 1522 (2003).

27. J. J. Burdett and C. J. Bardeen, J. Am. Chem. Soc. **134** (20), 8597 (2012).
https://doi.org/10.1021/ja301683w

28. Y. Inada, T. Yamao, M. Inada, et al., Synth. Met. **161** (17–18), 1869 (2011).
https://doi.org/10.1016/j.synthmet.2011.06.026

29. V. A. Postnikov, N. I. Sorokina, M. S. Lyasnikova, et al., Crystals **10**, 363 (2020).
https://doi.org/10.3390/cryst10050363

30. V. A. Postnikov, N. I. Sorokina, O. A. Alekseeva, et al., Crystallogr. Rep. **63** (1), 139 (2018).

31. V. A. Postnikov, N. I. Sorokina, A. A. Kulishov, et al., Acta Crystallogr. B **75**, 1076 (2019).
https://doi.org/10.1107/S2052520619012484

32. V. A. Postnikov, M. S. Lyasnikova, A. A. Kulishov, et al., Zh. Fiz. Khim. **93** (9), 1362 (2019).
https://doi.org/10.1134/s0044453719090188

33. V. A. Postnikov, Y. I. Odarchenko, A. V. Iovlev, et al., Cryst. Growth Des. **14** (4), 1726 (2014).
https://doi.org/10.1021/cg401876a

34. L. A. Nagahara, J. Vac. Sci. Technol. B: Microelectron. Nanom. Struct. **12** (3), 1694 (1994).
https://doi.org/10.1116/1.587265

35. D. Nečas and P. Klapetek, *Gwiddion Software: 2.59*.

36. M. Fulem, V. Lačtovka, M. Straka, et al., J. Chem. Eng. Data. **53** (9), 2175 (2008). https://doi.org/10.1021/je800382b

37. Y. Nagano, J. Chem. Thermodyn. **34** (3), 377 (2002). https://doi.org/10.1006/jcht.2001.0892

38. J. J. Burdett, A. M. Müller, D. Gosztola, et al., J. Chem. Phys. Am. Inst. Phys. **133** (14), 144506 (2010). https://doi.org/10.1063/1.3495764

39. F. H. Rhodes and F. S. Eisenhauer, Ind. Eng. Chem. **19** (3), 414 (1927). https://doi.org/10.1021/ie50207a028

40. A. Seidell, *Solubilities of Organic Compounds,* Vol. 2 (D. Van Nostrand Company, New York, 1941).

41. S. Walas, *Phase Equilibra in Chemical Engineering* (Elsevier, New York, 1981).

42. V. A. Rabinovich and Z. Ya. Khavin, *Brief Chemical Handbook* (Khimiya, Leningrad, 1978) [in Russian].

43. D. Holmes, S. Kumaraswamy, A. J. Matzger, et al., Chem. Eur. J. **5** (11), 3399 (1999). https://doi.org/10.1002/(SICI)1521-3765(19991105)5:11<3399::AID-CHEM3399>3.0.CO;2-V

44. Z. Zhang, G. Yu, J. Garcia-Barriocanal, et al., ACS Appl. Mater. Interfaces **12** (36), 40607 (2020). https://doi.org/10.1021/acsami.0c11566

45. *Mercury Software: 2021.1.0. CCDC.*

Translated by Yu. Sin'kov